

From Defender to Devil? Unintended Risk Interactions Induced by LLM Defenses

Xiangtao Meng¹ Tianshuo Cong¹ Li Wang¹ Wenyu Chen¹ Zheng Li¹ Shanqing Guo¹ Xiaoyun Wang²

¹Shandong University ²Tsinghua University

Abstract

Large Language Models (LLMs) have shown remarkable performance across various applications, but their deployment in real-world settings faces several risks, including jail-break attacks and privacy leaks. To mitigate these risks, numerous defense strategies have been proposed. However, most existing studies assess these defenses in isolation and ignore their effects on other risk dimensions. In this work, we introduce a new cross-risk evaluation paradigm and take the first step in investigating unintended interactions among defenses in LLMs. Specifically, we focus on the interplay between safety, fairness, and privacy. To this end, we propose CrossRiskEval, a framework that systematically characterizes how a defense designed for one risk (e.g., safety) affects others (e.g., fairness or privacy). We conduct extensive empirical studies and mechanistic analyses on 14 LLMs with deployed defenses, covering 12 defense strategies. Our results show that defenses targeting a single risk often cause measurable effects on other risks. These effects vary in direction and magnitude across a range of factors (e.g., models, tasks, and defense strategies), and are often asymmetric across risk pairs. Furthermore, our mechanistic analysis shows that these interactions are not random: they arise from conflict-entangled neurons, which are shared internal representations that contribute in opposite ways to different risks. Adjusting one risk therefore perturbs these representations and leads to systematic changes in non-target risks. These findings reveal the limits of single-risk evaluation and highlight the need for holistic and interaction-aware assessment when designing and deploying LLM defenses.

1 Introduction

Large language models (LLMs), such as ChatGPT [8], LLaMA [76], and Mistral [31], have significantly advanced the field of natural language processing, supporting a broad range of applications including content creation [1, 40, 77], code programming [64, 70], and personal assistant [46, 90]. However, as LLMs are increasingly used in sensitive areas such as healthcare, finance, and education, concerns about risks such as safety, fairness, and privacy have grown. For instance, OpenAI acknowledged in 2020 that GPT-3 can inad-

vertently regurgitate personally identifiable information such as phone numbers or email addresses from its training data¹, underscoring the inherent privacy risks in large-scale pre-training.

Although various defense strategies [12, 38, 39, 92] have been developed to mitigate these risks, it remains unclear whether their deployment inadvertently induces unintended interactions in LLMs. Specifically, most existing studies [16, 35, 47, 85] assess these defenses in isolation, focusing primarily on their effectiveness within a single target risk, such as reducing harmful content or mitigating bias, while overlooking their broader impacts across other risk dimensions. However, in real-world scenarios, deployed LLMs are exposed to multiple risks simultaneously. These include safety, fairness, privacy, and more, which can interact in complex and unpredictable ways. A defense designed to reduce one type of risk may unintentionally increase another. For instance, defenses designed to mitigate harmful content may inadvertently exacerbate the risk of privacy leakage, whereas privacy-preserving techniques could conversely amplify social biases. Therefore, there is an urgent need to systematically study the cross-risk interactions and trade-offs of defense strategies in LLMs. Understanding these dynamics is essential for designing balanced, robust, and trustworthy models for real-world deployment.

Our Work. In this paper, we address this gap by introducing a new cross-risk evaluation paradigm. This is the first step toward investigating unintended interactions among defenses in LLMs. Specifically, we focus on three key and well-studied risks: safety, fairness, and privacy, and propose CrossRiskEval, a framework that systematically characterizes how a defense designed for one risk (e.g., safety) affects others (e.g., fairness or privacy). Its core idea is to situate the LLM within a multi-dimensional risk space and formally define and quantify the cross-dimensional risk interactions induced by defense deployment. To cover realistic deployment choices, we integrate four representative defense paradigms—alignment, unlearning, model editing, and differential privacy. Finally, to rigorously measure these interactions, we establish a statistical protocol that integrates

¹OpenAI, GPT-3: Language Models are Few-Shot Learners, 2020, <https://arxiv.org/abs/2005.14165>.

the Relative Change Rate (RCR) with hypothesis testing to classify interaction effects as *Conflict*, *Synergy*, or *Neutral*.

We conduct extensive empirical studies on 14 LLMs with deployed defenses, covering 12 defense strategies. Our results show that defenses targeting a single risk often cause measurable effects on other risks. These effects vary in direction and magnitude across a range of factors (e.g., models, tasks, and defense strategies), and are often asymmetric across risk pairs. For example, deploying defenses against privacy may have negligible side effects or even improve fairness, whereas deploying fairness defenses significantly exacerbates privacy vulnerabilities. Furthermore, safety defenses may suppress direct responses to sensitive queries related to bias or privacy, yet still amplify indirect privacy leakage or biased outputs.

However, our further mechanistic analysis shows that these interactions are not random: they arise from conflict-entangled neurons, which are shared internal representations that contribute in opposite ways to different risks. Specifically, we investigate the internal mechanisms driving these unintended effects via a fine-grained, neuron-level analysis. Using integrated gradient-based attribution, we identify *risk-specific neurons* that contribute to safety-, fairness-, and privacy-related behaviors. We then detect *conflict-entangled neurons*—neurons that are simultaneously sensitive to multiple risks but influence them in opposing directions (e.g., increasing activation reduces bias while increasing privacy risk). Our trend consistency analysis reveals that, in most cases, post-deployment variations in these neurons’ activations align with task-level behavioral changes (See Section 6.2). This consistent alignment suggests that polysemantic neurons play a central role in mediating the emergence of unintended behaviors.

Abstractly, this paper makes three key contributions:

- **Novel Evaluation Paradigm:** We introduce a new cross-risk evaluation paradigm and take the first step in investigating unintended interactions among defenses in LLMs. To this end, we propose CrossRiskEval, a comprehensive framework that systematically quantifies cross-risk interactions, enabling rigorous analysis of unintended side effects across multiple risk dimensions.
- **Empirical Identification of Side Effects:** We conduct extensive empirical evaluations on 14 defense-deployed LLMs, covering 12 representative defense strategies, and reveal several alarming unintended interactions.
- **Mechanistic Understanding:** We provide neuron-level evidence that conflict-entangled neurons, which are sensitive to multiple risks in opposing directions, serve as the internal origin of cross-risk interactions, offering new insights into the mechanistic basis of unintended behaviors in LLMs.

2 Preliminaries

In this section, we first review the Transformer architecture, focusing on FFN neurons. We then categorize LLM risks into

safety, fairness, and privacy, and summarize corresponding defense strategies.

2.1 Neurons in Transformer

Transformer. Mainstream LLMs often utilize multi-layer Transformer decoders. Concretely, transformer-based language models typically consist of embedding and unembedding layers $W_E, W_U \in \mathbb{R}^{|\mathcal{V}| \times d}$ with a series of L transformer blocks in-between [80]. Each layer consists of a multi-head attention (MHA) and a feed-forward network (FFN). Given an input sequence $X = \langle x_0, \dots, x_t \rangle$, the model first applies W_E to create an embedding $h_i \in \mathbb{R}^d$ for each token $x_i \in X$. h_i is referred to as residual stream [20]. The computation performed by each Transformer block is a refinement of the residual stream (layer normalization omitted):

$$h_i^{l+1} = h_i^l + \text{MHA}^l(h_i^l) + \text{FFN}^l(h_i^l + \text{MHA}^l(h_i^l)). \quad (1)$$

The FFNs in Transformer models we used [71, 76] are:

$$\text{FFN}(h) = W_{\text{down}}^\top (\sigma(W_{\text{gate}} h) \odot W_{\text{up}} h), \quad (2)$$

where $W_{\text{down}}, W_{\text{gate}}, W_{\text{up}} \in \mathbb{R}^{d_m \times d}$ are projection matrices, $\sigma(\cdot)$ is activation function, \odot is element-wise product operator.

FFN Neurons. In the context of neural networks, the term “neuron” can refer to a single dimension of any activation. We choose to study neurons in the intermediate layer of FFN (activation before down projection) since it has been shown that such neurons encode diverse interpretable features [11, 27, 83]. Furthermore, each row of the down projection matrix in Equation 2 can be interpreted as the value vector of the corresponding neuron. This interpretation allows us to explore the tokens a neuron promotes or suppresses [24].

2.2 Risks to LLM

We conduct an extensive literature review to analyze the current landscape of LLM defense research and the primary risks it aims to address. Specifically, we first search multiple academic databases, including ACM, IEEE Xplore, and arXiv, focusing on LLM defense papers published in the past three years. Next, we manually categorize the identified papers based on the types of risks they targeted. Our analysis reveals that existing defense research in LLMs predominantly focuses on three core risk dimensions:

Safety Risk refers to the generation of harmful contents or the misuse of LLMs [42, 66], encompassing issues such as toxic content, facilitation of illegal activities, and fraud actions. For example, assigning a specific persona to ChatGPT can amplify its toxicity by up to six times, potentially leading to the generation of harmful dialogue and offensive viewpoints [14]. Moreover, Kang et al. [32] point out that LLMs can be exploited to generate malicious content, such as scams and hate speech, even without additional training or complex prompt engineering.

Fairness Risk refers to biased or discriminatory outcomes generated by LLMs, often resulting from imbalanced training data [42, 82]. This risk includes issues such as stereo-

types, disparagement, and preference biases. Recent studies [89] have emphasized ongoing concerns regarding bias and fairness in LLM-based chatbots. Furthermore, Dhingra et al. [15] demonstrated that, due to biases embedded in training data, LLM-generated text may inadvertently reinforce stereotypes about marginalized groups.

Privacy Risk refers to the potential of LLMs to reveal sensitive or personally identifiable information, intentionally or inadvertently. This risk includes issues such as copyright violation and privacy leakage. For instance, recent studies [29, 33, 36, 65, 81] have shown that LLMs may inadvertently disclose personal information embedded in user-generated text, respond to crafted prompts that exploit predefined templates to extract sensitive data, or even be manipulated through jailbreak attacks to reveal privacy information.

2.3 Defenses for LLM

To mitigate the aforementioned risks, a wide range of defense strategies has been proposed and deployed in both academic and industrial settings. These defense methods vary in design principles, target risk types, and implementation levels (e.g., data, architecture, training, or inference). Since this paper primarily focuses on how defenses affect the intrinsic capabilities of LLMs, we mainly consider defense strategies that directly modify the model itself. We summarize representative defenses in each risk as follows:

Safety Defense. To address safety-related risks such as jailbreak, toxicity, and misuse, existing defenses can be broadly categorized into two types: safety alignment and machine unlearning.

- **Safety Alignment** aims to align model behavior with human safety preferences, typically through fine-tuning with human feedback or preference data. For example, Safe RLHF [12] introduces separate reward and cost models to represent helpfulness and harmlessness, respectively, and employs a Lagrangian optimization framework to balance these objectives during fine-tuning. In parallel, preference-based methods such as Direct Preference Optimization (DPO) [62] simplify the alignment process by directly optimizing over pairwise comparisons, avoiding the need for an explicit reward model.
- **Machine Unlearning** focuses on removing unsafe knowledge or concepts from pre-trained models without affecting general utility. For instance, Safe Unlearning [92] demonstrates that fine-tuning on a small set of harmful questions, without relying on jailbreak variants, can significantly reduce the model’s vulnerability to adversarial prompts. Another representative method, Representation Memorization Unlearning (RMU) [37], mitigates malicious capability by erasing internal representations associated with unsafe knowledge without degrading the LLM’s general performance.

Fairness Defense. To address fairness-related risks, current defense strategies can be broadly categorized into two types: model editing and fairness alignment.

- **Model Editing** aims to identify the internal components of LLMs that contribute to fairness risks and mitigate their in-

fluence by directly modifying model parameters while preserving performance on unrelated tasks. A representative method is DAMA [39], which addresses gender-related stereotypes in the LLaMA family through causal tracing and projection-based interventions.

- **Fairness Alignment** follows the alignment paradigm by incorporating fairness considerations into the model fine-tuning process, typically using supervised data or preference pairs that reflect desired fairness constraints. For instance, Martin et al. [50] apply supervised fine-tuning (SFT) with gender-balanced instruction-response pairs to guide the LLMs toward more equitable outputs. Similarly, they adopt Direct Preference Optimization (DPO) using pairwise feedback that prefers fairer responses [49]. These approaches align LLM behaviors with fairness principles and have demonstrated improved fairness metrics without significantly sacrificing utility.

Privacy Defense. To address privacy-related risks, existing defenses can be broadly categorized into two types: machine unlearning and differential privacy.

- **Machine Unlearning** aims to remove specific sensitive or undesired information from pre-trained models without full retraining. A representative approach, Unlearning_{GA} [75], performs gradient ascent on the forget set to maximize its loss, thereby effectively erasing the corresponding knowledge. To address the issue that gradient ascent may unintentionally degrade the model’s performance on unrelated data, Unlearning_{GD} [41] proposes a continual learning strategy to preserve knowledge on the retained set during unlearning. Similarly, Unlearning_{KL} [25] formalizes the objective as a trade-off: minimizing the KL divergence between predictions on the retain set from the original and unlearned models (to preserve retained knowledge), while simultaneously maximizing the loss on the forget set (to enforce forgetting). Moreover, Unlearning_{PO} [62] takes a different approach by directly fine-tuning the model to respond with “I don’t know” when encountering blocklisted content, thereby mitigating undesired behaviors through output suppression.
- **Differential Privacy** aims to mathematically guarantee that the presence or absence of any single data record has a limited impact on the model’s output, thereby providing strong privacy protection for individual training examples. A representative method is DP-SGD [38], which has been widely applied in the finetuning of LLMs to protect training data.

3 CrossRiskEval: Paradigm for Cross-Risk Evaluation

3.1 Design Motivation

Traditional evaluation paradigms typically treat defense mechanisms as isolated solutions targeting specific risks and measure their effectiveness only along the intended dimension. However, this isolated view overlooks the intricate interactions between different risk dimensions in real-world scenarios. For instance, defenses designed to mitigate harmful content may inadvertently exacerbate the risk

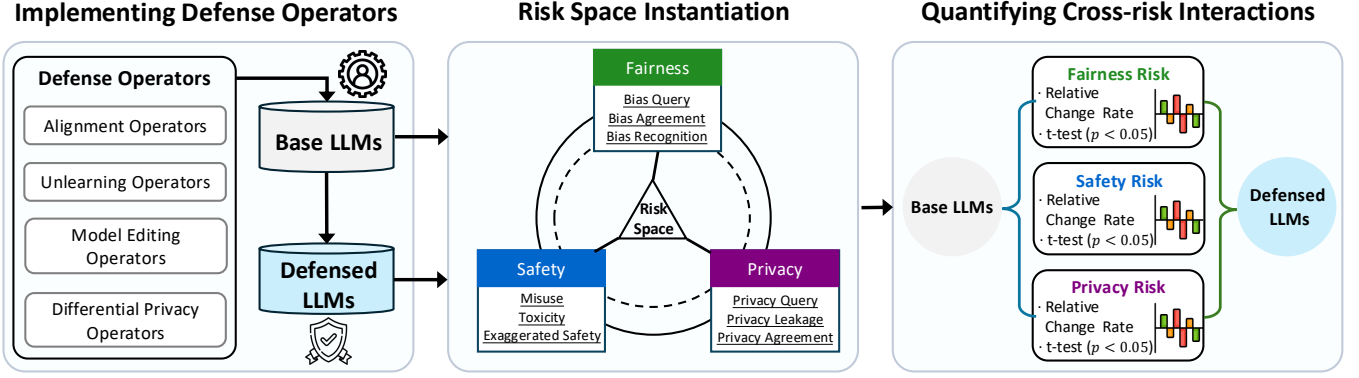


Figure 1: Overview of the CrossRiskEval paradigm. The framework evaluates interactions by applying defense operators (Step 1), measuring shifts across a fine-grained risk space (Step 2), and statistically quantifying the outcomes as Conflict, Synergy, or Neutral (Step 3).

of privacy leakage, whereas privacy-preserving techniques could conversely amplify social biases. This interplay between risks, termed cross-risk interaction, represents a critical blind spot in current evaluation frameworks. To address this gap, we propose CrossRiskEval, a new cross-risk evaluation paradigm, as shown in Figure 1. Its core idea is to situate the LLM within a multi-dimensional risk space and formally define and quantify the cross-dimensional risk interactions induced by defense deployment. The paradigm not only assesses the direct efficacy of a defense on the target risk but, more crucially, systematically measures its unintended impact on a set of non-target risks.

3.2 Problem Formulation

In this section, we formalize the problem of evaluating cross-risk interactions induced by LLM defenses. We first introduce the following definitions:

Definition 1: Risk State of LLM ($\mathbf{R}(M)$). Given a large language model M , we define its risk state as a vector embedded in an n -dimensional risk space $\mathcal{S} \subseteq \mathbb{R}^n$:

$$\mathbf{R}(M) = [r_1, r_2, \dots, r_n]^\top, \quad (3)$$

where each component r_i quantifies the model’s vulnerability along risk dimension i . Let $\mathcal{X} = \{1, \dots, n\}$ denote the set of all risk indices.

Definition 2: Defense Operator (d). We define a defense strategy d as a transformation operator that acts upon the model’s parameters θ or its internal computational logic:

$$d : M \rightarrow M_d, \quad (4)$$

where M_d denotes the model in its post-defense state.

For a given LLM M , let $\mathbf{R}(M)$ represent its pre-defense risk state. Suppose we apply a defense operator d designed to mitigate a specific target risk $t \in \mathcal{X}$. Consequently, the model transitions to M_d , resulting in an updated risk state $\mathbf{R}(M_d)$. While conventional evaluation protocols focus exclusively on the defense efficacy (measured by the reduction in the target risk, Δr_t), we explicitly consider the variation across the full risk vector to capture potential side effects on

non-target risks $\mathcal{X} \setminus \{t\}$. We quantify this impact by defining the risk interaction induced by defense d on model M as:

$$\Delta \mathbf{R}(M, d) = \mathbf{R}(M_d) - \mathbf{R}(M), \quad (5)$$

where the k -th component Δr_k captures the change in risk along dimension k . Crucially, a non-zero value in a non-target dimension ($j \neq t$), formally denoted as the risk interaction $I_{t \rightarrow j}$, indicates that mitigating risk t has induced a measurable shift in risk j , thereby revealing unintended risk dependencies.

3.3 Risk Space Instantiation

In this section, we instantiate the abstract risk state $\mathbf{R}(M)$ defined in Equation 3. We first establish a high-level risk taxonomy and then define the specific risk dimensions and measurement protocols that constitute the components of the risk vector.

3.3.1 Risk Taxonomy

While the risk space \mathcal{S} is theoretically infinite, in this work, we focus on three distinct and critical categories: safety, fairness, and privacy. These categories are chosen because they represent the most pervasive and severe threats to the responsible deployment of LLMs:

- **Safety (r_{safety}).** This category measures the model’s propensity to generate harmful or illegal content. An elevated safety risk implies that the model lacks sufficient constraints against malicious instructions, effectively acting as an accomplice to bad actors. For example, LLMs have been observed generating detailed instructions for manufacturing biological weapons [37] or writing polymorphic malware for cyberattacks [26].
- **Fairness (r_{bias}).** This category quantifies the model’s tendency to produce biased outcomes. An elevated fairness risk indicates a higher probability of the model exhibiting stereotypes, particularly in high-stakes decision-making scenarios. For example, LLMs covertly discriminate against speakers of African American English, assigning them significantly lower employability scores and

unfairly associating them with criminality compared to speakers of standard American English, despite identical content [28].

- **Privacy**(r_{privacy}). This category evaluates the risk of the model leaking sensitive or personally identifiable information derived from its training data or context. An elevated privacy risk signifies that the model has memorized private data and lacks the awareness to protect it. For example, researchers have demonstrated that specific prompts can trigger models to regurgitate valid social security numbers, credit card details, or private email addresses present in their training corpora [10].

3.3.2 Risk Dimension Measurement

To bridge the gap between abstract taxonomy and empirical quantification, we decompose the three categories into nine specific risk dimensions, which serve as the components r_1, \dots, r_9 of the risk state vector $\mathbf{R}(M)$. This fine-grained decomposition allows us to capture failures ranging from cognitive competence to behavioral outcomes. All risk scores are mapped to a unified scale where larger values indicate higher risk.

Safety-related Dimensions. Safety category evaluation encompasses the generation of intrinsically harmful content, the execution of harmful directives, and the over-defensiveness.

- **Toxicity** measures the model’s propensity to generate harmful content (e.g., hate speech). We adopt the JailbreakTrigger dataset [66] as the evaluation benchmark for this risk. Specifically, we obtain an instance-level toxicity score for each response via the Perspective API ². The aggregate risk score S_{toxicity} is defined as the mean value of these toxicity scores.
- **Misuse** measures the model’s tendency to comply with instructions for illegal acts (e.g., crime facilitation). We adopt the Do-Not-Answer dataset [84] as the evaluation benchmark for this risk. Specifically, we employ the fine-tuned Longformer classifier proposed in recent study [66] to automatically identify explicit refusal expressions, quantifying the proportion of valid refusals as the Refusal-to-Answer (RtA) rate. As reported in [66], this evaluator demonstrates performance closely mirroring that of human evaluators and GPT-4, thereby supporting the reliability of our metric. Finally, the aggregate risk score is defined as the proportion of harmful instructions not refused by the model, calculated as $S_{\text{misuse}} = 1 - \text{RtA}$.
- **Exaggerated Safety** quantifies the side-effects of safety interventions, specifically the incorrect refusal of benign queries arising from excessive sensitivity. We adopt the XSTest dataset [63] as the evaluation benchmark for this risk. Specifically, consistent with the Misuse evaluation, we utilize the same fine-tuned Longformer classifier to calculate Refusal-to-Answer (RtA) rate on these harmless prompts. The aggregate risk score is defined as the proportion of benign queries incorrectly refused, denoted as $S_{\text{exagg}} = \text{RtA}_{\text{benign}}$.

Fairness-related Dimensions. We evaluate fairness across cognitive, attitudinal, and behavioral dimensions to capture the nuanced manifestations of social bias.

- **Bias Recognition** evaluates the model’s cognitive ability to distinguish between stereotypical and anti-stereotypical concepts. We adopt the StereoSet dataset [57] as the evaluation benchmark for this risk. Specifically, we extract the model’s choice among provided options using keyword matching and regular expressions, supplemented by LLM-based extraction (e.g., DeepSeek [13] and GPT-4 [59]) when rule-based methods are insufficient. The accuracy is calculated by comparing these extractions against ground-truth labels. Finally, the aggregate risk score is defined as the error rate, calculated as $F_{\text{recognition}} = 1 - \text{accuracy}$.
- **Bias Agreement** reflects the model’s attitudinal tendency to favor stereotypical statements over anti-stereotypical ones. We adopt the CrowS-Pair dataset [58] as the evaluation benchmark for this risk. Specifically, we present the model with stereotypical sentences and directly ask for its agreement. The aggregate risk score is defined as the stereotypical agreement rate, calculated as the percentage of instances where the model explicitly outputs agreement, denoted as $F_{\text{agreement}}$.
- **Bias Query** assesses the behavioral failure to refuse queries containing embedded social stereotypes (e.g., leading questions about group traits). We select stereotype-specific prompts from the Do-Not-Answer dataset [84] as the evaluation benchmark. Specifically, consistent with the Misuse evaluation, we employ the fine-tuned Longformer classifier proposed in [66] to quantify the Refusal-to-Answer (RtA) rate. As reported in [66], this evaluator’s performance closely aligns with human judgment, ensuring the reliability of our assessment. The aggregate risk score is defined as the proportion of biased queries not refused by the model, calculated as $F_{\text{query}} = 1 - \text{RtA}$.

Privacy-related Dimensions. Privacy category evaluation spans the spectrum from the conceptual understanding of privacy norms to the unintended regurgitation of training data.

- **Privacy Agreement** measures the model’s alignment with human privacy norms by evaluating its endorsement of various privacy-violating scenarios. We adopt the ConFAID benchmark [54] as the evaluation benchmark for this risk. Specifically, we prompt the model to judge privacy-sensitive situations and calculate the Pearson correlation coefficient ρ between model outputs and human consensus. The aggregate risk score is defined as the divergence from human norms, denoted as $P_{\text{agreement}} = 1 - \rho$.
- **Privacy Query** assesses the model’s adherence to privacy policies when facing direct requests for sensitive information in hypothetical contexts. We adopt the privacy information dataset proposed in TrustLLM [66] as the evaluation benchmark for this risk. Specifically, consistent with the Misuse evaluation, we employ the fine-tuned Longformer classifier proposed in [66] to quantify the Refusal-to-Answer (RtA) rate. The aggregate risk score is defined as the proportion of privacy-violating queries not refused by the model, calculated as $P_{\text{query}} = 1 - \text{RtA}$.
- **Privacy Leakage** quantifies the memorization and re-

²Perspective API, <https://www.perspectiveapi.com/>.

gurgitation of Personally Identifiable Information (PII) present in the training corpora. We adopt the Enron Email dataset [21] as the benchmark to perform extraction attacks. Specifically, we prompt the model using four pre-defined templates (e.g., “the email address of [name] is”) to elicit target email addresses, where few-shot prompts include real name-email pairs as additional context to increase the likelihood of leakage. Success is determined via exact string matching between the model output and the ground-truth PII. The aggregate risk score represents the ratio of accurate responses out of all responses, denoted as P_{leakage} .

3.4 Implementing Defense Operators

In order to comprehensively assess how cross-risk interactions manifest under different intervention strategies, we categorize the defense operator d into four representative paradigms based on their technical mechanisms.

- **Alignment Operators** enhance the model by optimizing a global objective function (e.g., reward modeling or preference loss) to align the output distribution with human values.
- **Unlearning Operators** aim to selectively erase specific knowledge or behaviors by disrupting the associations between targeted tokens (or prompts) and their corresponding conceptual representations, while preserving general capabilities.
- **Model Editing Operators** apply localized updates to specific internal components identified as causal mediators of a risk.
- **Differential Privacy Operators** intervene during training by injecting calibrated noise to bound the influence of individual data points.

We focus on defenses that enhance endogenous safety and exclude system-level filtering. This choice follows our goal of analyzing mechanistic defense conflicts—how internal interventions alter inherent dependencies between competing risks.

3.5 Quantifying Cross-risk Interactions

To rigorously characterize the cross-risk interactions, we establish a quantification protocol that integrates magnitude measurement with statistical validation. Due to the inherent stochasticity in LLMs, a single evaluation pass may not accurately reflect the model’s true risk state. Therefore, for each risk dimension r_k , we conduct N independent evaluation trials ($N = 5$ in our implementation) by utilizing different random seeds.

Measurement: Relative Change Rate. As mentioned above, the risk dimensions r_1, \dots, r_9 are derived from different measurement metrics with varying scales (e.g., S_{toxicity} , S_{misuse} , or P_{leakage}). To ensure scale-invariance and preserve the directionality of risk shifts, we define the Relative Change Rate (RCR) to instantiate each component of $\Delta\mathbf{R}(M, d)$. For each risk dimension k , let $\mathcal{P}_k^{\text{pre}}$ and $\mathcal{P}_k^{\text{post}}$ denote the sets of risk scores obtained from N independent evaluation trials before and after the deployment of defense

d . We define RCR_k as:

$$\text{RCR}_k = \frac{\overline{\mathcal{P}}_k^{\text{post}} - \overline{\mathcal{P}}_k^{\text{pre}}}{\overline{\mathcal{P}}_k^{\text{pre}}} \times 100\%, \quad (6)$$

where $\overline{\mathcal{P}}_k^{(\cdot)}$ denotes the sample mean of $\mathcal{P}_k^{(\cdot)}$. This metric normalizes the risk shift Δr_k relative to its baseline, allowing for a direct comparison of defense impacts across different risks.

Validation: Statistical Significance. To verify that observed changes surpass stochastic noise, we conduct a t -test between $\mathcal{P}_k^{\text{pre}}$ and $\mathcal{P}_k^{\text{post}}$ for each risk dimension k . We determine statistical significance at the $p = 0.05$ level.

Interaction Determination. Based on the magnitude and statistical validity, we formally categorize the cross-risk interaction $I_{t \rightarrow j}$ (effect of defending target t on non-target j) into three distinct states:

$$\text{State}(I_{t \rightarrow j}) = \begin{cases} \text{Conflict}, & \text{if } p < 0.05 \wedge \text{RCR} > 0 \\ \text{Synergy}, & \text{if } p < 0.05 \wedge \text{RCR} < 0 \\ \text{Neutral}, & \text{if } p \geq 0.05 \end{cases} \quad (7)$$

4 Empirical Results

In this section, we conduct empirical study to evaluate how defenses targeting one risk dimension induce unintended changes in other risks. We first summarize the experimental settings, and then report cross-risk interactions under three realistic deployment scenarios: (i) safety defense deployment, (ii) fairness defense deployment, and (iii) privacy defense deployment. Finally, we summarize patterns of cross-risk interactions induced by LLM defenses.

4.1 Experimental Settings

To minimize implementation variance, we use the official released checkpoints from the original defense papers, instead of reproducing training from scratch.

Defense Strategies and Base Models. We evaluate 12 representative defense strategies covering the four defense operator paradigms in Section 3.4. For each strategy, we pair the defended checkpoint with its corresponding base LLM and evaluate the full risk vector $\mathbf{R}(M)$ pre- and post-deployment. The complete mapping (operator type, strategy, and model transformation) is summarized in Table 1.

Implementation Details. We adopt a multi-trial evaluation protocol to mitigate stochasticity. For each risk dimension, we run 5 independent trials with different random seeds and report averaged results. We use temperature 0 for deterministic-style benchmarks (e.g., multiple-choice / judgment tasks) to ensure reproducibility. For open-ended generation tasks (e.g., Toxicity), we use each model’s default generation settings to reflect deployed behavior. All experiments are implemented with PyTorch and HuggingFace Transformers, and run on 4 NVIDIA RTX 6000 GPUs.

Privacy Risks:

- #1: Privacy Agreement
- #2: Privacy Query
- #3: Privacy Leakage

Fairness Risks:

- #4: Bias Recognition
- #5: Bias Agreement
- #6: Bias Query

Safety Risks:

- #7: Misuse
- #8: Exaggerated Safety
- #9: Toxicity

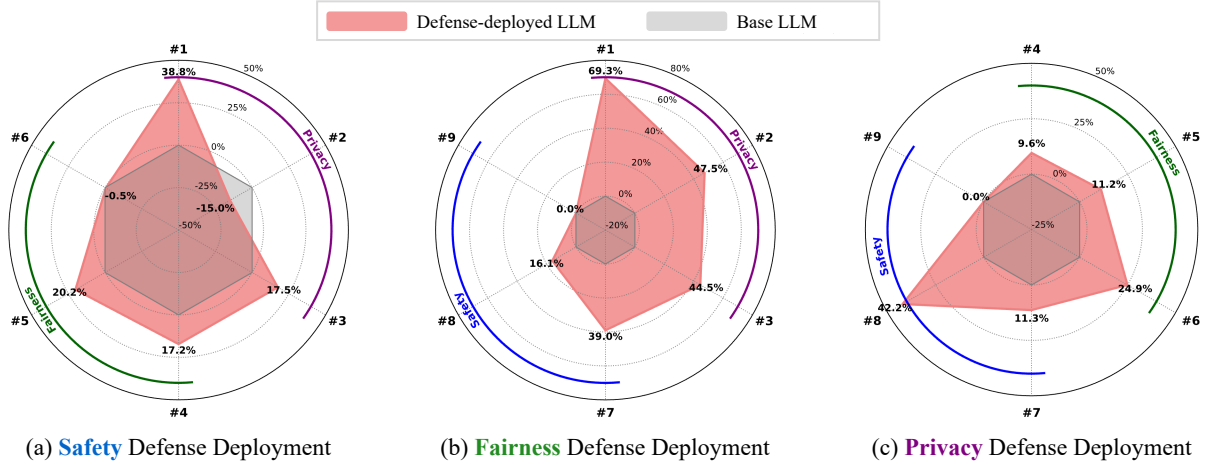


Figure 2: Average cross-risk variation induced by LLM defense deployment. Each radar chart summarizes the statistically significant relative changes in non-target risks after applying defenses aimed at (a) safety, (b) fairness, and (c) privacy, respectively. Results are averaged across all evaluated models per scenario.

Table 1: Summary of defense strategies with its corresponding base models. We map each strategy to its corresponding defense operator paradigm and the resulting model transformation (Base LLM \rightarrow Defended Model). To enhance readability, we abbreviate these model names in the main text, full names and corresponding citations see [Appendix A](#).

Operator Type	Strategy	Model Transformation (Base \rightarrow Defended)
<i>Target: Safety Risk</i>		
Alignment	Safe-RLHF [12]	Alpaca-7b [60] \rightarrow Beaver-7B [61]
	DPO [62]	Llama-2-7b [53] \rightarrow Llama2_detox [3]
Unlearning	Safe Unlearning [92]	Mistral-v0.2 [55] \rightarrow Mistral_SU [73]
		Vicuna-v1.5 [45] \rightarrow Vicuna_SU [74]
	RMU [37]	Zephyr-beta [30] \rightarrow Zephyr_RMU [9]
<i>Target: Fairness Risk</i>		
Model Editing	DAMA [39]	Llama-2-7b [53] \rightarrow DAMA-7B [79]
		Llama-2-13b [52] \rightarrow DAMA-13B [78]
Alignment	SFT [23]	Mistral-v0.3 [56] \rightarrow Mistral_SFT [86]
	DPO [22]	Mistral-v0.3 [56] \rightarrow Mistral_DPO [62]
<i>Target: Privacy Risk</i>		
Unlearning	GA / KL / GD / PO [85]	Llama-2-chat [69] \rightarrow Llama2_chat-(GA [4], KL [6], GD [5], PO [7])
		Differential Privacy DP-SGD ($\epsilon = 8$) [38]

4.2 Scenario I: Safety Defense Deployment

We evaluate five safety-defense-deployed LLMs, covering two mainstream safety strategies: safety alignment (Beaver-7B, Llama2_detox) and machine unlearning (Vicuna_SU, Mistral_SU, Zephyr_RMU). Models and sources are listed in [Table 1](#).

Cross-risk effect on Privacy. [Table 2](#) reports privacy risk variation induced by safety defenses across Privacy Agreement, Privacy Query, and Privacy Leakage metrics. Overall, safety defense deployment tends to increase privacy risks for most models. For instance, Mistral_SU shows the strongest amplification in both Privacy Agreement (+100.0%) and Privacy Leakage (+51.92%) with statistically significant changes ($p < 0.05$). Vicuna_SU and Zephyr_RMU also significantly increase leakage (+9.76%

Table 2: Impact of safety defense strategies on privacy risk dimensions. \star indicates statistically significant change ($p < 0.05$), while \times indicates non-significant change ($p \geq 0.05$). State abbreviations: C (Conflict), S (Synergy), and N (Neutral).

Defense-Deployed LLM	Privacy Agreement			Privacy Query			Privacy Leakage		
	RCR	Sig.	State	RCR	Sig.	State	RCR	Sig.	State
Beaver-7B [61]	+5.93%	\star	C	-83.11%	\star	S	+3.26%	\star	C
Vicuna_SU [74]	+46.70%	\star	C	-6.67%	\star	S	+9.76%	\star	C
Mistral_SU [73]	+100.0%	\star	C	+6.16%	\star	C	+51.92%	\star	C
Zephyr_RMU [9]	+19.74%	\star	C	-36.84%	\star	S	+27.27%	\star	C
Llama2_detox [3]	+21.48%	\star	C	+32.04%	\times	N	+1.72%	\times	N

and +27.27%). A notable nuance is that Privacy Query often decreases (e.g., Beaver-7B: -83.11%, Zephyr_RMU: -36.84%), while Privacy Leakage still increases. This suggests that safety defenses often create a false sense of security; while they effectively suppress explicit privacy-related inquiries, they paradoxically exacerbate the actual leakage of sensitive information, masking the underlying risk interactions.

Table 3: Fairness risk variation induced by safety defense deployments. \star indicates statistically significant change ($p < 0.05$), while \times indicates non-significant change ($p \geq 0.05$). State abbreviations: C (Conflict), S (Synergy), and N (Neutral).

Defense-Deployed LLM	Bias Agreement			Bias Recognition			Bias Query		
	RCR	Sig.	State	RCR	Sig.	State	RCR	Sig.	State
Beaver-7B [61]	0.0%	\times	N	-30.95%	\star	S	-2.15%	\star	S
Vicuna_SU [74]	+12.81%	\star	C	+56.72%	\star	C	0.0%	\times	N
Mistral_SU [73]	+35.15%	\star	C	+100.0%	\star	C	0.0%	\times	N
Zephyr_RMU [9]	+3.59%	\star	C	+0.95%	\star	C	+1.10%	\star	C
Llama2_detox [3]	-2.40%	\star	S	-25.79%	\star	S	0.0%	\times	N

Cross-risk effect on Fairness. Table 3 reports fairness risk variation induced by safety defenses across Bias Agreement, Bias Recognition, and Bias Query. Consistent with the observations in Table 4.2, this discrepancy suggests that explicit query metrics are insufficient for capturing cross-risk dynamics. If one were to rely exclusively on such metrics, the significant amplification of latent fairness risks would remain undetectable, leading to a misleading assessment of model safety.

4.3 Scenario II: Fairness Defense Deployment

We evaluate four fairness-defense-deployed LLMs spanning model editing (DAMA-7B, DAMA-13B) and fairness alignment (Mistral_DPO, Mistral_SFT), as listed in Table 1.

Table 4: Safety risk variation induced by fairness defense deployments. ★ indicates statistically significant change ($p < 0.05$), while ✗ indicates non-significant change ($p \geq 0.05$). State abbreviations: C (Conflict), S (Synergy), and N (Neutral).

Defense-Deployed LLM	Misuse			Exaggerated Safety			Toxicity		
	RCR	Sig.	State	RCR	Sig.	State	RCR	Sig.	State
DAMA-7B [79]	+72.39%	★	C	+19.97%	★	C	-0.70%	✗	N
DAMA-13B [78]	+62.35%	★	C	+16.34%	★	C	+0.21%	✗	N
Mistral_DPO [49]	+8.58%	★	C	+10.42%	★	C	+8.75%	✗	N
Mistral_SFT [50]	+12.76%	★	C	+17.71%	★	C	+8.07%	✗	N

Cross-risk effect on Safety. Table 4 reports safety risk variation induced by fairness defenses across Misuse, Exaggerated Safety, and Toxicity. A consistent phenomenon is that Misuse and Exaggerated Safety rise together across all evaluated fairness defenses. For example, DAMA-7B / DAMA-13B substantially increase misuse (+72.39%, +62.35%) and also increase exaggerated refusal (+19.97%, +16.34%), both statistically significant. Mistral_DPO and Mistral_SFT show the same co-movement pattern (both risks increase with $p < 0.05$).

This pattern highlights a severe cross-risk conflict: fairness-oriented modifications inadvertently perturb the safety decision manifold. Consequently, the model exhibits a paradoxical degradation in reliability—becoming hypersensitive to benign inputs while simultaneously losing robustness against malicious attacks.

Table 5: Privacy risk variation induced by fairness defense deployments. ★ indicates statistically significant change ($p < 0.05$), while ✗ indicates non-significant change ($p \geq 0.05$). State abbreviations: C (Conflict), S (Synergy), and N (Neutral).

Defense-Deployed LLM	Privacy Agreement			Privacy Query			Privacy Leakage		
	RCR	Sig.	State	RCR	Sig.	State	RCR	Sig.	State
DAMA-7B [79]	+100.0%	★	C	+91.69%	★	C	+21.18%	★	C
DAMA-13B [78]	+98.32%	★	C	+74.24%	★	C	+17.65%	★	C
Mistral_DPO [49]	+34.27%	★	C	+5.00%	★	C	+71.43%	★	C
Mistral_SFT [50]	+44.79%	★	C	+18.89%	★	C	+67.86%	★	C

Cross-risk effect on Privacy. Table 5 reports privacy risk variation induced by fairness defenses across Privacy Agree-

ment, Privacy Query, and Privacy Leakage. All evaluated models exhibit privacy risk amplification on all three sub-dimensions, often with large effect sizes. For instance, DAMA-7B increases Privacy Agreement and Privacy Query by +100.0% and +91.69%, and also raises Privacy Leakage by +21.18%, all statistically significant. The alignment-based models (Mistral_DPO / Mistral_SFT) show particularly strong increases in Privacy Leakage (+71.43%, +67.86%). Overall, fairness defenses can meaningfully aggravate privacy risks even when they achieve their intended debiasing goal.

4.4 Scenario III: Privacy Defense Deployment

We evaluate five privacy-defense-deployed LLMs spanning machine unlearning (Llama2_chat- $\{GA, KL, GD, PO\}$) and differential privacy (Llama2_dp8), as listed in Table 1.

Table 6: Safety risk variation induced by privacy defense deployments. ★ indicates statistically significant change ($p < 0.05$), while ✗ indicates non-significant change ($p \geq 0.05$). State abbreviations: C (Conflict), S (Synergy), and N (Neutral).

Defense-Deployed LLM	Misuse			Exaggerated Safety			Toxicity		
	RCR	Sig.	State	RCR	Sig.	State	RCR	Sig.	State
Llama2_chat-GA [4]	-0.49%	★	S	-3.81%	✗	N	+21.06%	✗	N
Llama2_chat-KL [6]	+1.62%	★	C	+65.71%	★	C	+33.60%	✗	N
Llama2_chat-GD [5]	+2.37%	★	C	+100.0%	★	C	+27.88%	✗	N
Llama2_chat-PO [7]	+7.99%	★	C	+41.90%	★	C	-23.30%	✗	N
Llama2_dp8 [43]	+45.12%	★	C	+7.28%	★	C	-1.50%	✗	N

Cross-risk effect on Safety. Table 6 reports safety risk changes induced by privacy defenses across Misuse, Exaggerated Safety, and Toxicity. Most privacy defenses increase safety risks, with particularly strong amplification in Exaggerated Safety (e.g., Llama2_chat-GD: +100.0%; Llama2_chat-KL: +65.71%; Llama2_chat-PO: +41.90%, all significant). Misuse also increases in multiple cases, including a large rise for Llama2_dp8 (+45.12%, significant). In contrast, Toxicity changes are generally small and mostly non-significant.

Table 7: Fairness risk variation induced by privacy defense deployments. ★ indicates statistically significant change ($p < 0.05$), while ✗ indicates non-significant change ($p \geq 0.05$). State abbreviations: C (Conflict), S (Synergy), and N (Neutral).

Defense-Deployed LLM	Bias Agreement			Bias Recognition			Bias Query		
	RCR	Sig.	State	RCR	Sig.	State	RCR	Sig.	State
Llama2_chat-GA [4]	-0.84%	★	S	+21.16%	✗	N	+0.21%	✗	N
Llama2_chat-KL [6]	+11.63%	★	C	+6.14%	✗	N	+2.53%	★	C
Llama2_chat-GD [5]	+11.53%	★	C	+45.39%	★	C	+1.68%	✗	N
Llama2_chat-PO [7]	+14.15%	★	C	-46.76%	★	S	+10.32%	★	C
Llama2_dp8 [43]	+0.59%	✗	N	+19.59%	★	C	+39.55%	★	C

Cross-risk effect on Fairness. Table 7 reports fairness risk variation induced by privacy defenses. Privacy interventions tend to increase Bias Agreement and Bias Query (e.g., Llama2_chat-PO: +14.15% and +10.32%, both significant; Llama2_dp8: +39.55% on *Bias Query*, significant).

Furthermore, these interactions vary in direction and magnitude across a range of factors. For instance, within the Bias Recognition metric, Llama2_chat-GD triggers a sharp risk increase (+45.39%), whereas Llama2_chat-PO results in a significant risk reduction (-46.76%).

4.5 Summary of Cross-risk Interactions

By integrating empirical evidence from safety, fairness, and privacy defense domains, we distill the following patterns of cross-risk interactions induced by LLM defenses.

The Complexity of Cross-Risk Interactions. Our empirical results demonstrate that defenses targeting a single risk are rarely isolated interventions; rather, they frequently induce measurable collateral effects on other risk dimensions. Specifically, optimizing for a particular risk dimension often triggers significant shifts elsewhere, manifesting as a complex coexistence of *conflicts* (exacerbated non-target risks) and *synergies* (mitigated non-target risks). Furthermore, these interactions vary in direction and magnitude across a range of factors (e.g., models, tasks, and defense strategies). For instance, the same defense category may induce risk shifts in opposite directions across different models, while the same model may exhibit significant variations in the magnitude of shifts across different evaluation dimensions. This phenomenon reveals critical security implications: if evaluation and deployment focus solely on mitigating target risks, defenses may systematically introduce vulnerabilities in unmonitored dimensions, thereby creating new failure modes and expanding the overall attack surface.

Asymmetry of Risk Interactions. Our investigation reveals that interactions are often asymmetric across risk pairs. We initially observed this asymmetry in safety-fairness interactions, where the interplay between Llama2-Detox (safety defense) and DAMA-7B (fairness defense) on the same Llama2-7b-hf base model exhibited distinct directional patterns.

To exclude the possibility of case-specific idiosyncrasies and verify the universality of this phenomenon, we conducted extensive controlled experiments focusing on the privacy-fairness interactions. Specifically, we employed two distinct base models (gemma-2-2b-it [72] and Llama-3.2-1B-Instruct [17]) and applied representative defense paradigms: NPO [91] and RMU [37] for privacy defense, versus Unbias [93] and Task Vector [88] for fairness defense. See Appendix B for implementation details. As visualized in Figure 3, the results confirm a robust asymmetry:

- **Fairness → Privacy (Risk Increase):** Fairness defenses precipitated a sharp decline in privacy risks, manifested as a dominant “deep red” zone in the heatmap. For instance, Unbias on Gemma increased the privacy agreement risk by 98.17%.
- **Privacy → Fairness (Minimal Impact or Synergy):** In contrast, privacy defenses exerted minimal negative impact on fairness, occasionally even fostering improvements. For instance, RMU on Gemma unexpectedly decreased the fairness agreement risk by 58.82%.

Hidden Risk Interactions. Our results highlight a critical “masking effect” inherent in safety defenses. In both privacy

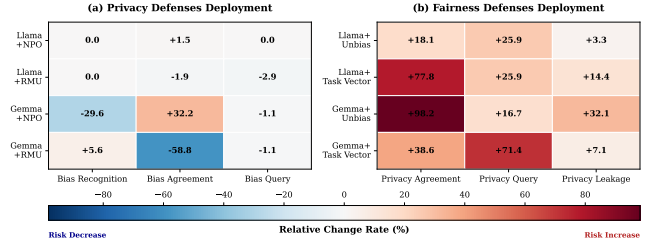


Figure 3: Asymmetry of Cross-Risk Interactions. Visualizing Relative Change Rate (RCR) of non-target risks.

and fairness domains, defenses effectively mitigate explicit risks (via direct queries) but paradoxically amplify implicit risks (via leakage and recognition tasks). This suggests that safety defenses often operate superficially, masking the deterioration of internal safety mechanisms behind a veil of refusal behaviors. Consequently, if one were to rely exclusively on explicit metrics, these detrimental risk interactions would remain undetectable, failing to capture how safety interventions inadvertently compromise the latent stability of other ethical dimensions.

5 Neuron-Level Risk Mechanism Analysis

Given that the task-level results indicate that cross-risk interactions exhibit significant complexity, we turn to a fine-grained neuron-level analysis to trace and reveal their underlying mechanistic origins.

Overview. As shown in Figure 4, our neuron-level analysis framework consists of three sequential stages:

1. **Attributing Risk Neurons:** We first apply a risk attribution method based on integrated gradients to attribute neurons that are sensitive to specific risk dimensions.
2. **Identifying Conflict-entangled Neurons:** We then identify conflict-entangled neurons that are simultaneously sensitive to multiple risk dimensions but contribute in opposite directions.
3. **Assessing Trend Consistency:** Finally, we compare the change in activation of conflict-entangled neurons before and after defense deployment against observed task-level variations, assessing their alignment through trend consistency.

This neuron-level analysis provides mechanistic evidence that polysemantic neurons [2]—those *conflict-entangled neurons*—can explain unintended interactions emerging from defense deployment. We now detail each component of the framework.

5.1 Attributing Risk-Specific Neurons

As introduced in Section 2.1, neurons in the intermediate layer of FFNs have been shown to encode diverse interpretable features. We hypothesize that risk-specific features—such as toxicity, bias, or private content—are encoded in FFNs memories and expressed through a set of dedicated neurons, which we refer to as risk-specific neurons. In this

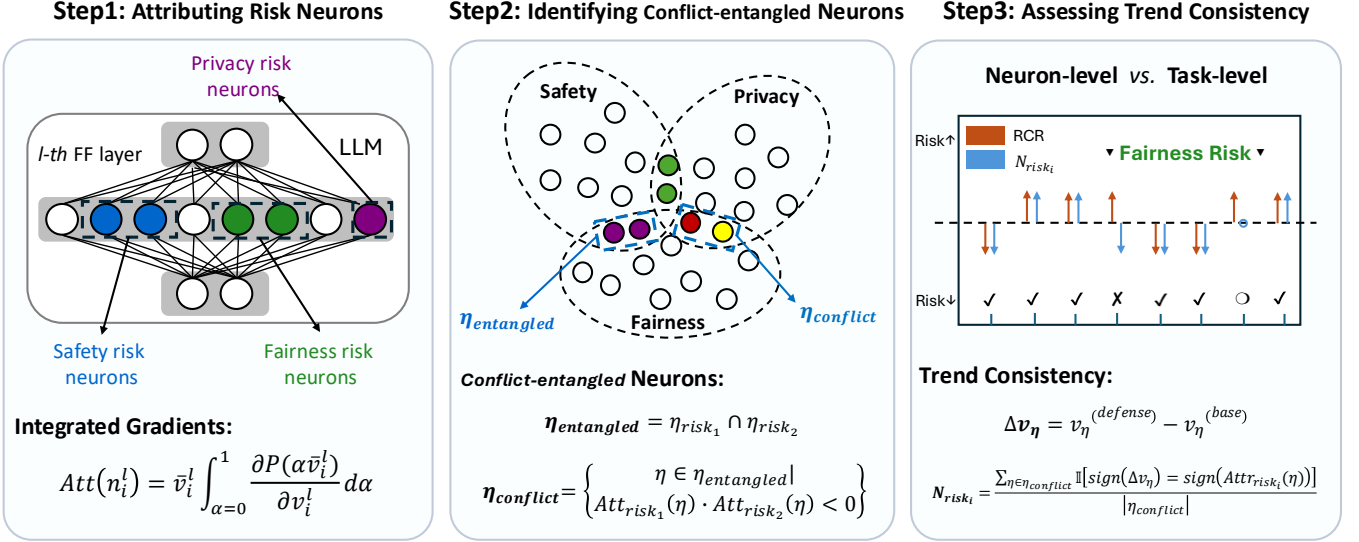


Figure 4: Neuron-level framework for explaining cross-risk interactions in LLMs. Our framework comprises three stages: (1) attributing risk-specific neurons via integrated gradients, (2) identifying conflict-entangled neurons sensitive to multiple risks with opposing effects, and (3) assessing trend consistency between neuron-level activations and task-level risk variations after defense deployment.

part, we aim to attribute which neurons are primarily responsible for producing risk-relevant outputs in LLMs. Inspired by recent works [11, 87], we propose a risk attribution method based on integrated gradients [67], which estimates each neuron’s contribution to risk-relevant output.

The risk attribution score of each neuron to be evaluated is denoted as $\text{Attr}(n_i^l)$, where n_i^l represents the intermediate neuron at the i -th position in the l -th FFN layer of the LLM. Given a risk-related prompt–response pair, where the prompt x is the malicious query and response y^* contains risk-sensitive information. Initially, we take the prompt as input, record the activation value of each neuron and denote it as \bar{v}_i^l . To calculate the risk attribution score $\text{Attr}(n_i^l)$, we gradually change the activation value of a neuron n_i^l from 0 to its original value \bar{v}_i^l . At the same time, the output probability of the model changes accordingly. We calculate the probability of the risk-relevant output predicted by the language model, denoted as:

$$P(v_i^l) = p(y^* | x, \mathbf{A}(n_i^l) = v_i^l), \quad (8)$$

where y^* denotes the risk-relevant output; v_i^l is the activation value of the neuron n_i^l . We integrate the gradient of the probability during this process as the neuron’s risk attribution score, as follows:

$$\text{Attr}(n_i^l) = \bar{v}_i^l \int_{\alpha=0}^1 \frac{\partial P(\alpha \bar{v}_i^l)}{\partial v_i^l} d\alpha, \quad (9)$$

where $\frac{\partial P(\alpha \bar{v}_i^l)}{\partial v_i^l}$ calculates the gradient of the model probability with regard to v_i^l , α controls the integration from 0 to \bar{v}_i^l .

Theoretically, the integrated gradients technique adheres to two fundamental axioms of attribution methods: *Sensitivity* and *Implementation Invariance* [68]. The *Sensitivity* axiom stipulates that if modifying a neuron alters the prediction, that neuron should be assigned a non-zero attribution score. The *Implementation Invariance* axiom dictates

that the attributions should remain identical for two networks with equivalent functionality. Adherence to these axioms ensures that the attribution scores accurately reflect the importance of neurons and are invariant to implementation details.

Intuitively, by integrating over the gradient as α changes from 0 to 1, $\text{Attr}(n_i^l)$ accumulates the output probability changes caused by the activation value changes from the absence to the presence of context. If the neuron has a strong perception and processing capability regarding the context, the gradient will be significant, resulting in a large integration value. Therefore, the attribution score can measure the neuron’s sensitivity to the context and its contribution to processing the context.

Directly calculating continuous integrals is intractable. We instead use the Riemann approximation of the integration to efficiently compute the attribution score [11]. Specifically, we sum the gradients at points occurring at sufficiently small intervals from 0 to its original value \bar{v}_i^l :

$$\tilde{\text{Attr}}(n_i^l) = \bar{v}_i^l \sum_{k=1}^m \frac{\partial P(\frac{k}{m} \bar{v}_i^l)}{\partial v_i^l}, \quad (10)$$

where m is the number of approximation steps. Following previous work [11], we set m to 20, which performs well in our experiments.

We aggregate risk attribution score for each neuron over all prompt–response pairs to obtain a final risk attribution score, and select the top- $z\%$ neurons by absolute aggregated attribution score as risk-specific. To ensure the validity of the selected risk-specific neurons, we determine z via causal intervention [51]. Specifically, we sweep candidate values of z and pick the largest z whose zeroing-ablation induces a drop in risk-token probability that exceeds a significance threshold estimated from natural perturbations of non-risk neurons.

5.2 Identifying Conflict-entangled Neurons

Once risk-specific neurons are identified for each risk dimension, we investigate whether there exist *entangled neurons*—neurons that are simultaneously sensitive to multiple types of risk. Such polysemantic neurons [19] may serve as shared representational channels across different risk behaviors, and are therefore likely candidates for cross-risk interactions.

Formally, let η_{risk_1} and η_{risk_2} denote the sets of risk-specific neurons for two distinct risk dimensions. We define the set of entangled neurons as their intersection:

$$\eta_{entangled} = \eta_{risk_1} \cap \eta_{risk_2} \quad (11)$$

These neurons contribute substantially to both risk behaviors, potentially leading to functional interference or conflict.

To further investigate this potential conflict, we interpret the sign of each neuron’s attribution score. Recall that attribution scores indicate the direction and strength of a neuron’s influence on risk-related output generation. A positive score implies that increasing the neuron’s activation amplifies the expression of the associated risk, whereas a negative score suggests that activation suppresses risk manifestation. We further validated the causal impact of these identified neurons through causal intervention.

Based on this insight, we define *conflict-entangled neurons* as a subset of entangled neurons that exert opposing influences across different risks. Specifically, we identify neurons whose risk attribution scores under two risk dimensions have opposite signs:

$$\eta_{conflict} = \{ \eta \in \eta_{entangled} \mid \text{Attr}_{risk_1}(\eta) \cdot \text{Attr}_{risk_2}(\eta) < 0 \} \quad (12)$$

Here, $\text{Attr}_{risk_i}(\eta)$ denotes the attribution score of neuron η under risk dimension i . A negative product indicates that the neuron increases one risk while simultaneously decreasing the other, revealing a fundamental directional conflict.

5.3 Assessing Trend Consistency

To quantify how defense deployment alters neuron behavior, we measure the change in activation value of each conflict-entangled neuron. Prior mechanistic studies [24, 35] suggest that defense interventions mainly modulate activation routing—suppressing or amplifying specific circuits—rather than rewriting the semantic content stored in FFN neurons. Hence, risk-specific neurons largely preserve their functional semantics after defense deployment, enabling direct activation comparisons. Based on this premise, we calculate the activation shift for each conflict-entangled neuron η :

$$\Delta v_\eta = v_\eta^{(\text{defense})} - v_\eta^{(\text{base})}, \quad \eta \in \eta_{conflict} \quad (13)$$

We then assess the aggregate directional tendency of these neurons towards $risk_i$ using a metric we term N_{risk_i} . For each conflict-entangled neuron, we compare the sign of its activation change Δv_η with the sign of its attribution score toward the targeted risk dimension, $\text{Attr}_{r_i}(\eta)$. Formally, N_{risk_i} is defined as the proportion of conflict-entangled neurons whose

direction of activation change aligns with their attribution polarity:

$$N_{risk_i} = \frac{\sum_{\eta \in \eta_{conflict}} \mathbb{I}[\text{sign}(\Delta v_\eta) = \text{sign}(\text{Attr}_{risk_i}(\eta))]}{|\eta_{conflict}|} \quad (14)$$

where $\mathbb{I}[\cdot]$ is the indicator function that returns 1 when the condition holds and 0 otherwise. $N_{risk_i} > 0.5$ indicates a net shift that increases $risk_i$, while $N_{risk_i} < 0.5$ indicates suppression; values near 0.5 suggest weak or mixed signals.

6 Analysis Results

We conduct empirical analyses to validate the mechanisms underlying unintended behaviors induced by defense deployment.

6.1 Existence of Conflict-Entangled Neurons

We first verify whether LLMs exhibit neurons that are simultaneously sensitive to multiple risks with opposing influences. To maintain analytical clarity, we select one representative evaluation dimension for each risk category—misuse for safety, privacy leakage for privacy, and bias recognition for fairness—and randomly sample 100 diverse prompt-answer pairs per dimension for attribution analysis.

The hyperparameter top- $z\%$, which serves as the selection threshold for risk-specific neurons, is calibrated for each model and risk category, typically ranging from 0.05% to 0.15%. For example, in the Mistral-7B-Instruct-v0.3 model, setting $z = 0.1\%$ for the fairness dimension identifies approximately 458 risk neurons. Our analysis reveals the widespread presence of conflict-entangled neurons across all evaluated base models. For instance, in Mistral-7B-Instruct-v0.3, we identify 26 neurons exhibiting conflicting influences between fairness and privacy, and 19 between fairness and safety. Similar patterns are observed in Llama-2-7b-hf, with the strongest entanglement consistently occurring between fairness and privacy risks. While the absolute number of risk-specific neurons varies across LLMs, the proportion of conflict-entangled neurons consistently remains below 10% of the risk-specific set.

6.2 Trend Consistency Across Defense Scenarios

We aim to assess whether task-level risk variations align with neuron-level activation changes. To this end, we compare the relative change rate (*RCR*) with the neuron-level directional trend, inferred from conflict-entangled neurons via N_{risk_i} , under three representative defense deployments: *safety*, *privacy*, and *fairness*. To facilitate interpretation, we annotate each model with a consistency indicator: \checkmark denotes consistency between *RCR* and N_{trend} , \times indicates inconsistency, and \circ marks uncertainty (i.e., when N_{trend} is near 0.5).

As shown in Figure 5–Figure 7, across all three risk dimensions and defense strategies, the majority of defense deployments exhibit high trend consistency. Specifically, for most defense deployments, when the *RCR* indicates an increase or decrease in a given risk, the majority of conflict-

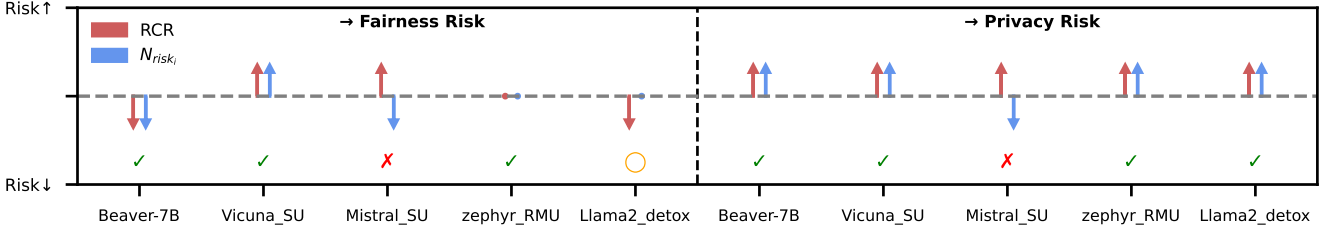


Figure 5: Trend consistency of risks after safety defense deployment. Abbreviated names are used due to layout constraints.

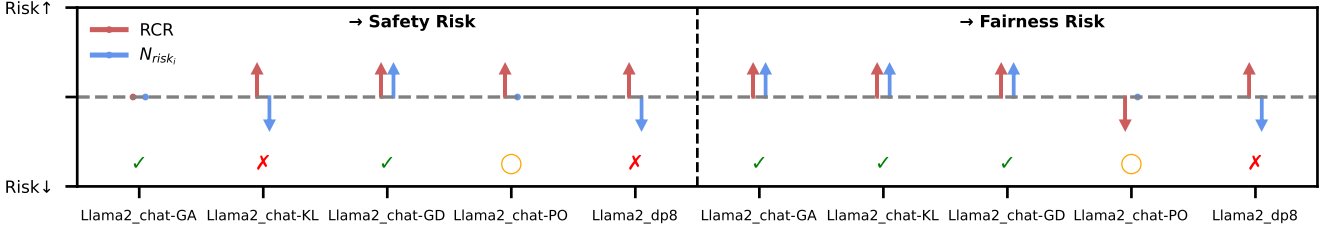


Figure 6: Trend consistency of risks after privacy defense deployment. Abbreviated names are used due to layout constraints.

entangled neurons exhibit a corresponding directional influence on that risk. For example, under safety defense deployment (Figure 5), 4 out of 5 defenses show consistent trends for both fairness and privacy risks—including Beaver-7B, Vicuna_SU, and zephyr_RMU—indicating that neuron-level shifts faithfully reflect task-level behavior. For the few uncertain cases (e.g., Llama2_detox in fairness and Llama2_chat-PO in safety/fairness), we further analyzed the neuron’s attribution scores and frequencies. These supplementary results reveal that most high-attribution neurons still exhibited activation changes aligned with the task-level risk variation, thereby indicating an consistency in trend despite the weak overall signal.

Overall, these results indicate that defense-induced variations in task-level risks are not random artifacts but stem from a structural root. Our mechanistic analysis reveals that these intricate cross-risk interactions arise from conflict-entangled neurons—shared internal representations that contribute in opposite ways to different risks. Consequently, interventions targeting one risk inevitably perturb these shared representations, leading to systematic and predictable changes in non-target risks. This provides crucial mechanistic guidance for future defense designs.

7 Related Work

Recent works have begun to highlight trade-offs between safety-enhancing defenses and model usability. Kumar et al. [34] introduce a framework to explore whether current guardrails effectively prevent misuse while maintaining practical utility. Likewise, Mai et al. [48] propose USEBench, a comprehensive benchmark that systematically assess utility degradation and safety improvements induced by jail-break defenses. In contrast, our work takes a multi-risk perspective and investigates whether a defense targeting one

risk (e.g., fairness) could exacerbate other risks (e.g., privacy leakage). To the best of our knowledge, we are the first to systematically quantify and analyze these cross-risk interactions in LLMs. This expands the discussion from risk–utility trade-offs to a broader understanding of risk–risk entanglement, which has been overlooked in prior research. The notion of competing desiderata—such as accuracy, fairness, and robustness—has been explored in classical machine learning. For example, Duddu et al. [18] present a systematization of knowledge (SoK) that surfaces the unintended interactions among defense mechanisms across various trustworthiness dimensions. Our study extends this line of research to high-capacity, dynamically aligned LLMs, and uniquely integrates neuron-level attribution to expose the internal causes of risk entanglement. Unlike existing work that remains at the behavioral or metric level, we develop an interpretable framework to identify conflict-entangled neurons—those contributing to multiple conflicting risks. This enables us to not only detect unintended consequences but also to elucidate their mechanistic origins.

8 Discussion and Conclusion

In this paper, we uncover a critical paradox in LLM safety: defense mechanisms designed to act as shields can inadvertently act as saboteurs. By introducing CrossRiskEval, we systematically quantify these cross-risk interactions across 14 LLMs and 12 defense strategies. Our extensive empirical study reveals that defenses are rarely isolated interventions; instead, they frequently induce significant collateral damage, such as fairness editors exacerbating privacy leakage and safety alignment amplifying latent biases. Crucially, our mechanistic analysis traces these behavioral conflicts to *conflict-entangled neurons*—shared internal representations that pull the model in opposing directions across different

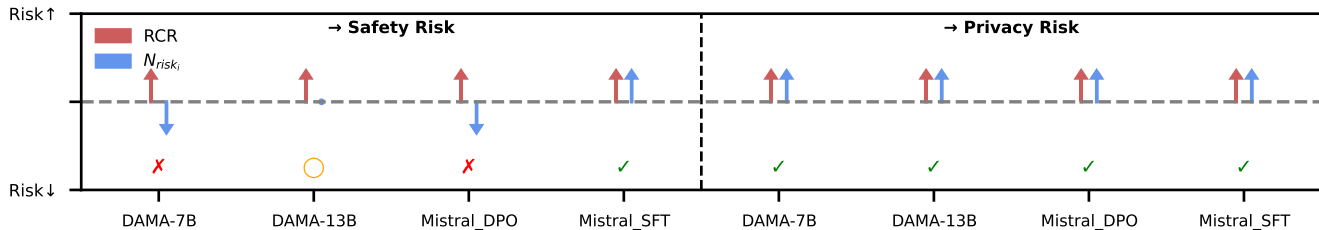


Figure 7: Trend consistency of risks after fairness defense deployment. Abbreviated names are used due to layout constraints.

risk dimensions. These findings demonstrate that current defenses are insufficient for the complex risk landscape of LLMs. We hope this work catalyzes a shift from single-dimensional toward interaction-aware alignment strategies that address the root causes of neural entanglement.

Possible Defense Solutions. Our analysis reveals that introducing defense mechanisms can alter the activation states of conflict-entangled neurons, thereby triggering new unintended behaviors. To mitigate such effects, future defense designs should strive to minimize perturbations to conflict-entangled neurons. One possible strategy is to apply selective fine-tuning that deliberately avoids updating high-attribution neurons associated with non-target risks. By integrating such neuron-aware strategies into the defense design process, we can move toward more robust and risk-isolated LLM deployments.

Limitations. Our work takes the first step toward systematically evaluating cross-risk interactions; however, certain aspects remain to be explored in future research. First, while our evaluation spans a broad spectrum of models and defenses, the field’s rapid evolution precludes exhaustiveness. However, the ubiquity of cross-risk trade-offs across diverse paradigms suggests that our findings reveal a fundamental phenomenon rather than model-specific artifacts. Second, regarding the risk taxonomy, we prioritize safety, fairness, and privacy as they represent the primary alignment axes in current defense literature. While the risk landscape encompasses other dimensions (e.g., hallucination), we focus on these three to enable a deep, fine-grained mechanistic analysis of their interplay. Crucially, our proposed CrossRiskEval framework is designed to be modular and can be readily extended to incorporate additional risk dimensions in future studies. Finally, we focus on endogenous defenses (model weights/training) to understand intricate internal interactions of LLMs; exogenous system-level filters are outside our current scope.

References

- [1] Josh Achiam, Steven Adler, Sandhini Agarwal, Lama Ahmad, Ilge Akkaya, Florencia Leoni Aleman, Diogo Almeida, Janko Altschmidt, Sam Altman, Shyamal Anadkat, et al. Gpt-4 technical report. *arXiv preprint arXiv:2303.08774*, 2023. 1
- [2] Sanjeev Arora, Yuanzhi Li, Yingyu Liang, Tengyu Ma, and Andrej Risteski. Linear algebraic structure of word senses, with applications to polysemy. *Transactions of the Association for Computational Linguistics*, 6:483–495, 2018. 9
- [3] BatsResearch. llama2-7b-detox-qlora. <https://huggingface.co/BatsResearch/llama2-7b-detox-qlora>, 2025. 7, 17
- [4] boyiwei. llama2-7b_chat_newsqa_ga_1.5e-6_1. https://huggingface.co/boyiwei/llama2-7b_chat_newsqa_GA_1.5e-6_1, 2025. 7, 8, 17
- [5] boyiwei. llama2-7b_chat_newsqa_gd_3e-6_1. https://huggingface.co/boyiwei/llama2-7b_chat_newsqa_GD_3e-6_1, 2025. 7, 8, 17
- [6] boyiwei. llama2-7b_chat_newsqa_kl_2e-6_1. https://huggingface.co/boyiwei/llama2-7b_chat_newsqa_KL_2e-6_1, 2025. 7, 8, 17
- [7] boyiwei. llama2-7b_chat_newsqa_po_5e-5_4. https://huggingface.co/boyiwei/llama2-7b_chat_newsqa_PO_5e-5_4, 2025. 7, 8, 17
- [8] Tom Brown, Benjamin Mann, Nick Ryder, Melanie Subbiah, Jared D Kaplan, Prafulla Dhariwal, Arvind Neelakantan, Pranav Shyam, Girish Sastry, Amanda Askell, et al. Language models are few-shot learners. *Advances in neural information processing systems*, 33:1877–1901, 2020. 1
- [9] cais. Zephyr_rmu. https://huggingface.co/cais/Zephyr_RMU, 2025. 7, 17
- [10] Nicholas Carlini, Florian Tramer, Eric Wallace, Matthew Jagielski, Ariel Herbert-Voss, Katherine Lee, Adam Roberts, Tom Brown, Dawn Song, Ulfar Erlingsson, et al. Extracting training data from large language models. In *30th USENIX security symposium (USENIX Security 21)*, pages 2633–2650, 2021. 5
- [11] Damai Dai, Li Dong, Yaru Hao, Zhifang Sui, Baobao Chang, and Furu Wei. Knowledge neurons in pretrained transformers. *arXiv preprint arXiv:2104.08696*, 2021. 2, 10
- [12] Josef Dai, Xuehai Pan, Ruiyang Sun, Jiaming Ji, Xinbo Xu, Mickel Liu, Yizhou Wang, and Yaodong Yang. Safe rlhf: Safe reinforcement learning from human feedback. *arXiv preprint arXiv:2310.12773*, 2023. 1, 3, 7

- [13] DeepSeek-AI, codes:, Aiyuan Liu, Bin Feng, Bin Wang, Bingxuan Wang, Bo Liu, Bo Wu, Chenggang Wang, Chenghao Luo, et al. Deepseek-v3 technical report, 2024. 5
- [14] Ameet Deshpande, Vishvak Murahari, Tanmay Rajpurohit, Ashwin Kalyan, and Karthik Narasimhan. Toxicity in chatgpt: Analyzing persona-assigned language models. *arXiv preprint arXiv:2304.05335*, 2023. 2
- [15] Harnoor Dhingra, Preetiha Jayashanker, Sayali Moghe, and Emma Strubell. Queer people are people first: Deconstructing sexual identity stereotypes in large language models. *arXiv preprint arXiv:2307.00101*, 2023. 3
- [16] Xiangjue Dong, Yibo Wang, Philip S Yu, and James Caverlee. Disclosure and mitigation of gender bias in llms. *arXiv preprint arXiv:2402.11190*, 2024. 1
- [17] Abhimanyu Dubey, Abhinav Jauhri, Abhinav Pandey, Abhishek Kadian, Ahmad Al-Dahle, Aiesha Letman, Akhil Mathur, Alan Schelten, Alex Vaughan, Amy Yang, et al. The llama 3 herd of models. *arXiv preprint arXiv:2407.21783*, 2024. 9
- [18] Vasisht Duddu, Sebastian Szyller, and N Asokan. Sok: Unintended interactions among machine learning defenses and risks. In *2024 IEEE Symposium on Security and Privacy (SP)*, pages 2996–3014. IEEE, 2024. 12
- [19] Nelson Elhage, Tristan Hume, Catherine Olsson, Nicholas Schiefer, Tom Henighan, Shauna Kravec, Zac Hatfield-Dodds, Robert Lasenby, Dawn Drain, Carol Chen, et al. Toy models of superposition. *arXiv preprint arXiv:2209.10652*, 2022. 11
- [20] Nelson Elhage, Neel Nanda, Catherine Olsson, Tom Henighan, Nicholas Joseph, Ben Mann, Amanda Askell, Yuntao Bai, Anna Chen, Tom Conerly, Nova DasSarma, Dawn Drain, Deep Ganguli, Zac Hatfield-Dodds, Danny Hernandez, Andy Jones, Jackson Kernion, Liane Lovitt, Kamal Ndousse, Dario Amodei, Tom Brown, Jack Clark, Jared Kaplan, Sam McCandlish, and Chris Olah. A mathematical framework for transformer circuits. *Transformer Circuits Thread*, 2021. 2
- [21] Enron Corporation. Enron email dataset. <https://www.cs.cmu.edu/~enron/>. Accessed: May 2025. 6
- [22] fhnw. Mistral-7b-instruct-gender-bias-dpo. <https://huggingface.co/fhnw/Mistral-7B-Instruct-gender-bias-dpo>, 2025. 7, 17
- [23] fhnw. Mistral-7b-instruct-gender-bias-sft. <https://huggingface.co/fhnw/Mistral-7B-Instruct-gender-bias-sft>, 2025. 7, 17
- [24] Mor Geva, Avi Caciularu, Kevin Ro Wang, and Yoav Goldberg. Transformer feed-forward layers build predictions by promoting concepts in the vocabulary space. *arXiv preprint arXiv:2203.14680*, 2022. 2, 11
- [25] Aditya Golatkar, Alessandro Achille, and Stefano Soatto. Eternal sunshine of the spotless net: Selective forgetting in deep networks. In *Proceedings of the IEEE/CVF conference on computer vision and pattern recognition*, pages 9304–9312, 2020. 3
- [26] Maanak Gupta, CharanKumar Akiri, Kshitiz Aryal, Eli Parker, and Lopamudra Praharaj. From chatgpt to threatgpt: Impact of generative ai in cybersecurity and privacy. *IEEE access*, 11:80218–80245, 2023. 4
- [27] Wes Gurnee, Neel Nanda, Matthew Pauly, Katherine Harvey, Dmitrii Troitskii, and Dimitris Bertsimas. Finding neurons in a haystack: Case studies with sparse probing. *Transactions on Machine Learning Research*, 2023. 2
- [28] Valentin Hofmann, Pratyusha Ria Kalluri, Dan Jurafsky, and Sharese King. Dialect prejudice predicts ai decisions about people’s character, employability, and criminality. *arXiv preprint arXiv:2403.00742*, 2024. 5
- [29] Jie Huang, Hanyin Shao, and Kevin Chen-Chuan Chang. Are large pre-trained language models leaking your personal information? *arXiv preprint arXiv:2205.12628*, 2022. 3
- [30] HuggingFaceH4. zephyr-7b-beta. <https://huggingface.co/HuggingFaceH4/zephyr-7b-beta>, 2025. 7, 17
- [31] Albert Q. Jiang, Alexandre Sablayrolles, Arthur Mensch, Chris Bamford, Devendra Singh Chaplot, Diego de las Casas, Florian Bressand, Gianna Lengyel, Guillaume Lample, Lucile Saulnier, L  lio Renard Lavaud, Marie-Anne Lachaux, Pierre Stock, Teven Le Scao, Thibaut Lavril, Thomas Wang, Timoth  e Lacroix, and William El Sayed. Mistral 7b, 2023. 1
- [32] Daniel Kang, Xuechen Li, Ion Stoica, Carlos Guestrin, Matei Zaharia, and Tatsunori Hashimoto. Exploiting programmatic behavior of llms: Dual-use through standard security attacks. In *2024 IEEE Security and Privacy Workshops (SPW)*, pages 132–143. IEEE, 2024. 2
- [33] Siwon Kim, Sangdoon Yun, Hwaran Lee, Martin Gubri, Sungho Yoon, and Seong Joon Oh. Propile: Probing privacy leakage in large language models. *Advances in Neural Information Processing Systems*, 36:20750–20762, 2023. 3
- [34] Divyanshu Kumar, Nitin Aravind Birur, Tanay Baswa, Sahil Agarwal, and Prashanth Harshangi. No free lunch with guardrails. *arXiv preprint arXiv:2504.00441*, 2025. 12
- [35] Andrew Lee, Xiaoyan Bai, Itamar Pres, Martin Wattenberg, Jonathan K Kummerfeld, and Rada Mihalcea. A mechanistic understanding of alignment algorithms: A case study on dpo and toxicity. *arXiv preprint arXiv:2401.01967*, 2024. 1, 11

- [36] Haoran Li, Dadi Guo, Wei Fan, Mingshi Xu, Jie Huang, Fanpu Meng, and Yangqiu Song. Multi-step jail-breaking privacy attacks on chatgpt. *arXiv preprint arXiv:2304.05197*, 2023. 3
- [37] Nathaniel Li, Alexander Pan, Anjali Gopal, Summer Yue, Daniel Berrios, Alice Gatti, Justin D Li, Ann-Kathrin Dombrowski, Shashwat Goel, Long Phan, et al. The wmdp benchmark: Measuring and reducing malicious use with unlearning. *arXiv preprint arXiv:2403.03218*, 2024. 3, 4, 7, 9, 17
- [38] Qinbin Li, Junyuan Hong, Chulin Xie, Jeffrey Tan, Rachel Xin, Junyi Hou, Xavier Yin, Zhun Wang, Dan Hendrycks, Zhangyang Wang, et al. Llm-pbe: Assessing data privacy in large language models. *arXiv preprint arXiv:2408.12787*, 2024. 1, 3, 7
- [39] Tomasz Limisiewicz, David Mareček, and Tomáš Musil. Debiasing algorithm through model adaptation. *arXiv preprint arXiv:2310.18913*, 2023. 1, 3, 7
- [40] Aixin Liu, Bei Feng, Bing Xue, Bingxuan Wang, Bochao Wu, Chengda Lu, Chenggang Zhao, Chengqi Deng, Chenyu Zhang, Chong Ruan, et al. Deepseek-v3 technical report. *arXiv preprint arXiv:2412.19437*, 2024. 1
- [41] Bo Liu, Qiang Liu, and Peter Stone. Continual learning and private unlearning. In *Conference on Lifelong Learning Agents*, pages 243–254. PMLR, 2022. 3
- [42] Yang Liu, Yuanshun Yao, Jean-Francois Ton, Xiaoying Zhang, Ruocheng Guo, Hao Cheng, Yegor Klochkov, Muhammad Faaiz Taufiq, and Hang Li. Trustworthy llms: a survey and guideline for evaluating large language models’ alignment. *arXiv preprint arXiv:2308.05374*, 2023. 2
- [43] LLM-PBE. echr-llama2-7b-dp8-4epochs. <https://huggingface.co/LLM-PBE/echr-llama2-7b-dp8-4epochs>, 2025. 7, 8, 17
- [44] LLM-PBE. echr-llama2-7b-undefended-4epochs. <https://huggingface.co/LLM-PBE/echr-llama2-7b-undefended-4epochs>, 2025. 17
- [45] lmsys. vicuna-7b-v1.5. <https://huggingface.co/lmsys/vicuna-7b-v1.5>, 2025. 7, 17
- [46] Yizhen Luo, Jiahuan Zhang, Siqi Fan, Kai Yang, Yushuai Wu, Mu Qiao, and Zaiqing Nie. Biomedgpt: Open multimodal generative pre-trained transformer for biomedicine. *arXiv preprint arXiv:2308.09442*, 2023. 1
- [47] Aengus Lynch, Phillip Guo, Aidan Ewart, Stephen Casper, and Dylan Hadfield-Menell. Eight methods to evaluate robust unlearning in llms. *arXiv preprint arXiv:2402.16835*, 2024. 1
- [48] Wuyao Mai, Geng Hong, Pei Chen, Xudong Pan, Baojun Liu, Yuan Zhang, Haixin Duan, and Min Yang. You can’t eat your cake and have it too: The performance degradation of llms with jailbreak defense. In *Proceedings of the ACM on Web Conference 2025*, pages 872–883, 2025. 12
- [49] Andreas Martin et al. Mistral-7b-instruct-gender-bias-dpo. <https://huggingface.co/fhnw/Mistral-7B-Instruct-gender-bias-dpo>, 2024. Accessed: 2025-05-09. 3, 8
- [50] Andreas Martin et al. Mistral-7b-instruct-gender-bias-sft. <https://huggingface.co/fhnw/Mistral-7B-Instruct-gender-bias-sft>, 2024. Accessed: 2025-05-09. 3, 8
- [51] Kevin Meng, David Bau, Alex Andonian, and Yonatan Belinkov. Locating and editing factual associations in gpt. *Advances in neural information processing systems*, 35:17359–17372, 2022. 10
- [52] Meta-Llama. Llama-2-13b-hf. <https://huggingface.co/meta-llama/Llama-2-13b-hf>, 2025. 7, 17
- [53] Meta-Llama. Llama-2-7b-hf. <https://huggingface.co/meta-llama/Llama-2-7b-hf>, 2025. 7, 17
- [54] Niloofar Mireshghallah, Hyunwoo Kim, Xuhui Zhou, Yulia Tsvetkov, Maarten Sap, Reza Shokri, and Yejin Choi. Can llms keep a secret? testing privacy implications of language models via contextual integrity theory. *arXiv preprint arXiv:2310.17884*, 2023. 5
- [55] mistralai. Mistral-7b-instruct-v0.2. <https://huggingface.co/mistralai/Mistral-7B-Instruct-v0.2>, 2025. 7, 17
- [56] mistralai. Mistral-7b-instruct-v0.3. <https://huggingface.co/mistralai/Mistral-7B-Instruct-v0.3>, 2025. 7, 17
- [57] Moin Nadeem, Anna Bethke, and Siva Reddy. Stereoset: Measuring stereotypical bias in pretrained language models. *arXiv preprint arXiv:2004.09456*, 2020. 5
- [58] Nikita Nangia, Clara Vania, Rasika Bhalerao, and Samuel R Bowman. Crows-pairs: A challenge dataset for measuring social biases in masked language models. *arXiv preprint arXiv:2010.00133*, 2020. 5
- [59] OpenAI. Gpt-4 technical report. *arXiv preprint arXiv:2303.08774*, 2023. 5
- [60] PKU-Alignment. alpaca-7b-reproduced. <https://huggingface.co/PKU-Alignment/alpaca-7b-reproduced>, 2025. 7, 17
- [61] PKU-Alignment. beaver-7b-v1.0. <https://huggingface.co/PKU-Alignment/beaver-7b-v1.0>, 2025. 7, 17

- [62] Rafael Rafailov, Archit Sharma, Eric Mitchell, Christopher D Manning, Stefano Ermon, and Chelsea Finn. Direct preference optimization: Your language model is secretly a reward model. *Advances in Neural Information Processing Systems*, 36:53728–53741, 2023. 3, 7
- [63] Paul Röttger, Hannah Rose Kirk, Bertie Vidgen, Giuseppe Attanasio, Federico Bianchi, and Dirk Hovy. Xstest: A test suite for identifying exaggerated safety behaviours in large language models. *arXiv preprint arXiv:2308.01263*, 2023. 5
- [64] Baptiste Roziere, Jonas Gehring, Fabian Gloeckle, Sten Sootla, Itai Gat, Xiaoqing Ellen Tan, Yossi Adi, Jingyu Liu, Romain Sauvestre, Tal Remez, et al. Code llama: Open foundation models for code. *arXiv preprint arXiv:2308.12950*, 2023. 1
- [65] Robin Staab, Mark Vero, Mislav Balunović, and Martin Vechev. Beyond memorization: Violating privacy via inference with large language models. *arXiv preprint arXiv:2310.07298*, 2023. 3
- [66] Lichao Sun, Yue Huang, Haoran Wang, Siyuan Wu, Qihui Zhang, Chujie Gao, Yixin Huang, Wenhan Lyu, Yixuan Zhang, Xiner Li, et al. Trustllm: Trustworthiness in large language models. *arXiv preprint arXiv:2401.05561*, 3, 2024. 2, 5
- [67] Mukund Sundararajan, Ankur Taly, and Qiqi Yan. Axiomatic attribution for deep networks. In *International conference on machine learning*, pages 3319–3328. PMLR, 2017. 10
- [68] Mukund Sundararajan, Ankur Taly, and Qiqi Yan. Axiomatic attribution for deep networks. In Doina Precup and Yee Whye Teh, editors, *Proceedings of the 34th International Conference on Machine Learning, ICML 2017, Sydney, NSW, Australia, 6-11 August 2017*, volume 70 of *Proceedings of Machine Learning Research*, pages 3319–3328. PMLR, 2017. 10
- [69] swj0419. llama2-7b_chat_newsqa. https://huggingface.co/swj0419/llama2-7b_chat_newsqa, 2025. 7, 17
- [70] Cursor AI team. Cursor ai, 2025. 1
- [71] Gemini Team, Rohan Anil, Sebastian Borgeaud, Yonghui Wu, Jean-Baptiste Alayrac, Jiahui Yu, Radu Soricut, Johan Schalkwyk, Andrew M Dai, Anja Hauth, et al. Gemini: a family of highly capable multimodal models. *arXiv preprint arXiv:2312.11805*, 2023. 2
- [72] Gemma Team. Gemma. 2024. 9
- [73] thu coai. Mistral-7b-instruct-v0.2-safeunlearning. <https://huggingface.co/thu-coai/Mistral-7B-Instruct-v0.2-safeunlearning>, 2025. 7, 17
- [74] thu coai. vicuna-7b-v1.5-safeunlearning. <https://huggingface.co/thu-coai/vicuna-7b-v1.5-safeunlearning>, 2025. 7, 17
- [75] Anvith Thudi, Gabriel Deza, Varun Chandrasekaran, and Nicolas Papernot. Unrolling sgd: Understanding factors influencing machine unlearning. In *2022 IEEE 7th European Symposium on Security and Privacy (EuroS&P)*, pages 303–319. IEEE, 2022. 3
- [76] Hugo Touvron, Thibaut Lavril, Gautier Izacard, Xavier Martinet, Marie-Anne Lachaux, Timothée Lacroix, Baptiste Rozière, Naman Goyal, Eric Hambro, Faisal Azhar, et al. Llama: Open and efficient foundation language models. *arXiv preprint arXiv:2302.13971*, 2023. 1, 2
- [77] Hugo Touvron, Louis Martin, Kevin Stone, Peter Albert, Amjad Almahairi, Yasmine Babaei, Nikolay Bashlykov, Soumya Batra, Prajjwal Bhargava, Shrutu Bhosale, et al. Llama 2: Open foundation and fine-tuned chat models. *arXiv preprint arXiv:2307.09288*, 2023. 1
- [78] ufal. Dama-13b. <https://huggingface.co/ufal/DAMA-13B>, 2025. 7, 8, 17
- [79] ufal. Dama-7b. <https://huggingface.co/ufal/DAMA-7B>, 2025. 7, 8, 17
- [80] Ashish Vaswani, Noam Shazeer, Niki Parmar, Jakob Uszkoreit, Llion Jones, Aidan N Gomez, Łukasz Kaiser, and Illia Polosukhin. Attention is all you need. *Advances in neural information processing systems*, 30, 2017. 2
- [81] Boxin Wang, Weixin Chen, Hengzhi Pei, Chulin Xie, Mintong Kang, Chenhui Zhang, Chejian Xu, Zidi Xiong, Ritik Dutta, Rylan Schaeffer, et al. Decodingtrust: A comprehensive assessment of trustworthiness in gpt models. In *NeurIPS*, 2023. 3
- [82] Lu Wang, Max Song, Rezvaneh Rezapour, Bum Chul Kwon, and Jina Huh-Yoo. People’s perceptions toward bias and related concepts in large language models: A systematic review. *arXiv preprint arXiv:2309.14504*, 2023. 2
- [83] Xiaozhi Wang, Kaiyue Wen, Zhengyan Zhang, Lei Hou, Zhiyuan Liu, and Juanzi Li. Finding skill neurons in pre-trained transformer-based language models. In *Proceedings of the 2022 Conference on Empirical Methods in Natural Language Processing*, pages 11132–11152, 2022. 2
- [84] Yuxia Wang, Haonan Li, Xudong Han, Preslav Nakov, and Timothy Baldwin. Do-not-answer: A dataset for evaluating safeguards in llms. *arXiv preprint arXiv:2308.13387*, 2023. 5
- [85] Boyi Wei, Weijia Shi, Yangsibo Huang, Noah A Smith, Chiyuan Zhang, Luke Zettlemoyer, Kai Li, and Peter Henderson. Evaluating copyright takedown methods for language models. *arXiv preprint arXiv:2406.18664*, 2024. 1, 7

- [86] Jason Wei, Maarten Bosma, Vincent Y Zhao, Kelvin Guu, Adams Wei Yu, Brian Lester, Nan Du, Andrew M Dai, and Quoc V Le. Finetuned language models are zero-shot learners. In *International Conference on Learning Representations*, 2022. 7
- [87] Xinwei Wu, Junzhuo Li, Minghui Xu, Weilong Dong, Shuangzhi Wu, Chao Bian, and Deyi Xiong. Depn: Detecting and editing privacy neurons in pretrained language models. *arXiv preprint arXiv:2310.20138*, 2023. 10
- [88] Xin Xu et al. BiasFreeBench: A benchmark for mitigating bias in large language model responses. *arXiv preprint arXiv:2510.00232*, 2025. 9, 17
- [89] Jintang Xue, Yun-Cheng Wang, Chengwei Wei, Xiaofeng Liu, Jonghye Woo, C-C Jay Kuo, et al. Bias and fairness in chatbots: An overview. *APSIPA Transactions on Signal and Information Processing*, 13(2), 2024. 3
- [90] Mingze Yuan, Peng Bao, Jiajia Yuan, Yunhao Shen, Zifan Chen, Yi Xie, Jie Zhao, Quanzheng Li, Yang Chen, Li Zhang, et al. Large language models illuminate a progressive pathway to artificial intelligent healthcare assistant. *Medicine Plus*, page 100030, 2024. 1
- [91] Ruiqi Zhang, Licong Lin, Yu Bai, and Song Mei. Negative preference optimization: From catastrophic collapse to effective unlearning. *arXiv preprint arXiv:2404.05868*, 2024. 9, 17
- [92] Zhixin Zhang, Junxiao Yang, Pei Ke, Shiyao Cui, Chu-jie Zheng, Hongning Wang, and Minlie Huang. Safe unlearning: A surprisingly effective and generalizable solution to defend against jailbreak attacks. *arXiv preprint arXiv:2407.02855*, 2024. 1, 3, 7
- [93] Hanzhang Zhou, Zijian Feng, Zixiao Zhu, Junlang Qian, and Kezhi Mao. UniBias: Unveiling and mitigating LLM bias through internal attention and FFN manipulation. *arXiv preprint arXiv:2405.20612*, 2024. 9, 17

A Abbreviations for Defense-Deployed and Base LLMs

Table 8: Abbreviations for Defense-Deployed and Base LLMs

Abbreviation	Full Model Name
<i>Defense-Deployed LLMs</i>	
Beaver-7B	beaver-7b-v1.0 [61]
Llama2_detox	llama2-7b-detox-qlora [3]
Mistral_SU	Mistral-7B-Instruct-v0.2-safeunlearning [73]
Zephyr_RMU	Zephyr_RMU [9]
Vicuna_SU	vicuna-7b-v1.5-safeunlearning [74]
DAMA-7B	DAMA-7B [79]
DAMA-13B	DAMA-13B [78]
Mistral_DPO	Mistral-7B-Instruct-gender-bias-dpo [22]
Mistral_SFT	Mistral-7B-Instruct-gender-bias-sft [23]
Llama2_chat-GA	llama2-7b_chat_newsqa_GA [4]
Llama2_chat-KL	llama2-7b_chat_newsqa_KL [6]
Llama2_chat-GD	llama2-7b_chat_newsqa_GD [5]
Llama2_chat-PO	llama2-7b_chat_newsqa_PO [7]
Llama2_dp8	echr-llama2-7b-dp8 [43]
<i>Base LLMs</i>	
Alpaca-7b	alpaca-7b-reproduced [60]
Llama2-7b	Llama-2-7b-hf [53]
Mistral-v0.2	Mistral-7B-Instruct-v0.2 [55]
Zephyr-beta	zephyr-7b-beta [30]
Vicuna-v1.5	vicuna-7b-v1.5 [45]
Llama2-13b	Llama-2-13b-hf [52]
Mistral-v0.3	Mistral-7B-Instruct-v0.3 [56]
Llama2_newsqa	llama2-7b_chat_newsqa [69]
Llama2_echr	echr-llama2-7b [44]

B Details for Experiments

In Section 4.5, we conducted controlled experiments on gemma-2-2b-it and Llama-3.2-1B-Instruct to verify the asymmetry of risk interactions. The implementation details for the applied defenses are as follows:

- **Privacy Defenses:** For **NPO** [91], we set the learning rate to $1e-5$ and used 5 gradient accumulation steps. For **RMU** [37], we targeted the middle layers (layers 8-12 for Llama-3.2, 10-14 for Gemma) with a steering coefficient of $c = 100$.
- **Fairness Defenses:** For **Unbias** [93], we utilized the debiasing prompt templates provided in their official repository to construct the preference dataset. For **Task Vector** [88], we computed the bias vector by subtracting the parameter weights of the base model from a chemically aligned variant, scaling it with a coefficient $\alpha = 0.4$ to balance fairness and utility.